Pergamon

0042-6989(94)00203-7

Vision Res. Vol. 35, No. 7, pp. 999–1010, 1995

0042-6989/95 $9.50 + 0.00

A Reflectometric Technique for Assessing Photoreceptor Alignment

JEAN-MARIE GORRAND,*† FRANÇOIS DELORI*

Received 16 April 1993; in revised form 14 July 1994

Clinical studies of photoreceptor orientation are limited by the fact that psychophysical methods for measuring the Stiles–Crawford effect are time consuming and require excellent co-operation from the subject. We have developed a novel instrument, the photoreceptor alignment reflectometer (PAR), that determines photoreceptor alignment by measuring the distribution in the pupil of light reflected by one retinal location. This determination is accomplished in a measurement time of 4 sec and requires minimal co-operation from the subject. The technique is not significantly affected by reflections at the limiting membrane, or by changes in entrance and exit pupil configuration, or by location of bleaching light entry. The PAR was used to measure the orientation of foveal photoreceptors, their directionality, and the ratio of directional to diffuse flux in 20 normal subjects ranging in age from 20 to 60 yr.

Alignment Fovea Orientation Photoreceptor Reflectometer

INTRODUCTION

The photoreceptors at the posterior pole are oriented towards the centre of the pupil (Enoch & Hope, 1973; Bedell & Enoch, 1979). This orientation, together with the waveguide properties of photoreceptors is responsible for the Stiles–Crawford effect (i.e. the eye is more sensitive for light entering the pupil along photoreceptor axes). This ideal arrangement of photoreceptors was shown to be disturbed in numerous clinical situations, including retinitis pigmentosa (Birch, Sandberg & Berson, 1982; Bailey, Lakshminarayanan & Enoch, 1991), central serous choroidopathy (Smith, Pokorny & Diddie, 1978), gyrate atrophy (Yasuma, Hamer, Lakshminarayanan, Enoch & O'Donnell, 1986), fibrous scars (Pokorny, Smith & Johnston, 1979), trauma (Campos, Bedell, Enoch & Fitzgerald, 1978) and age-related macular changes (Fitzgerald, Enoch, Campos & Bedell, 1979; Smith, Pokorny & Diddie, 1988). Clinical measurement of the Stiles–Crawford function is time-consuming, requires excellent co-operation from the subject, and is therefore limited to a restricted number of patients. To address these limitations, Gorrand (1985, 1989) and van Blokland (1986) introduced reflectometric methods to determine *in vivo* the orientation of human photoreceptors.

We have developed a novel technique, the photoreceptor alignment reflectometer (PAR), that determines photoreceptor alignment by measuring the distribution in the pupil of light reflected by one retinal location (Gorrand & Delori, 1990). This determination is accomplished in a measurement time of 4 sec and requires minimal co-operation from the subject. In this paper we describe the principles and the technical realization of the PAR, experimentally investigate possible non-photoreceptor contributions, and present results from 20 normal subjects ranging in age from 20 to 60 yr.

METHODS

Principles

Enoch (1961) could observe modal patterns inside photoreceptors. A consequence of this waveguide behaviour is that a lightbeam incident upon a photoreceptor launches bound modes. Under natural viewing conditions, a photoreceptor receives rays coming from the entire subject pupil; using an artificial pupil of small dimension (entrance pupil) allows us to select a single direction of incidence. For an entrance pupil close to photoreceptor axes, a large fraction of incoming light is guided along photoreceptors (Snyder, 1969), then radiated from outer segment tips into the retinal pigment epithelium. Light backscattered from layers scleral to photoreceptors can be collected by outer segments, guided backwards along photoreceptors, then radiated from myoid towards the subject's pupil. The reciprocity theorem of optics predicts that the geometric cone into which light is radiated (from the myoid to the pupil) is identical to the cone from which the myoid accepts light (from the pupil). An artificial pupil of small dimension (exit pupil) allows us to select a single direction of collection. The radiant flux collected through the

*The Schepens Eye Research Institute, 20 Staniford Street, Boston, MA 02114, U.S.A.
†Present address: Faculty of Medicine, Biomathematics, B.P. 38, 63001 Clermont-Ferrand, France [*Fax* 33 7326 9990].

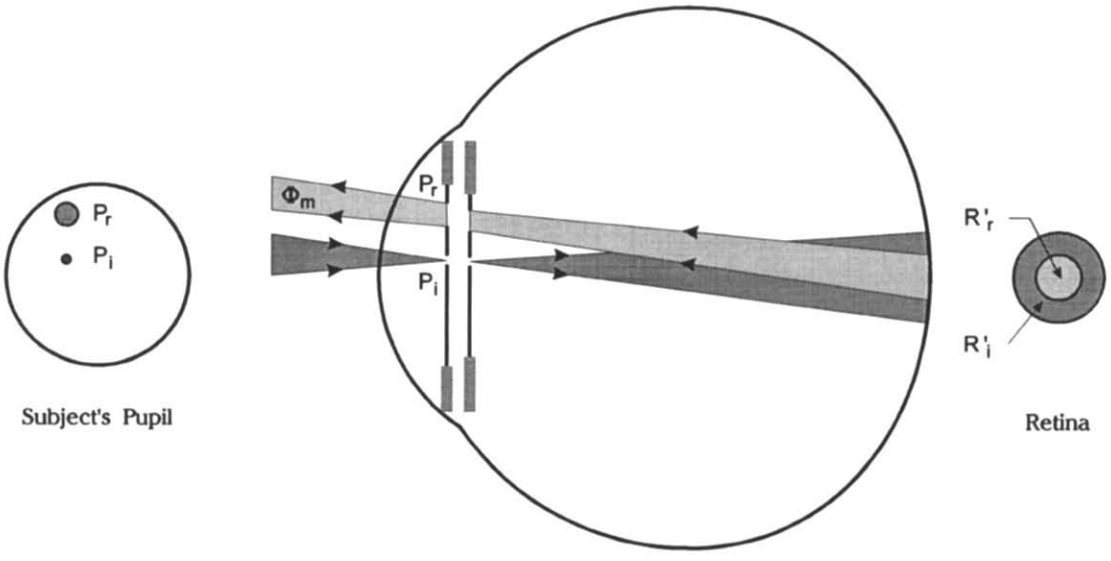

FIGURE 1. *Principle.* Light enters the eye through the entrance pupil P_i (dia <0.1 mm). R_i' determines the retinal area which is illuminated, R_r' the photoreceptor population which is tested. The radiant flux Φ_m collected by the exit pupil P_r (dia: 1 mm) is measured by a photomultiplier.

exit pupil is maximal for an exit pupil centred on photoreceptor axes; it decreases when the exit pupil edges away from photoreceptor axes.

Figure 1 presents the method. Light enters the eye through the entrance pupil P_i (dia <0.1 mm) and illuminates a retinal field R_i'. The reflected light is sampled from a field R_r' and is collected through the exit pupil P_r (dia: 1 mm). The radiant flux Φ_m passing through P_r is measured by a photomultiplier (PMT). In our instrument, entrance pupil P_i (centre J) and exit pupil P_r (centre G) are moved jointly in the subject's pupil (centre O, Fig. 2). This is accomplished with stationary retinal fields (R_i' and R_r'). The position of H, the midpoint between J and G, is defined by the co-ordinates x (horizontal axis) and y (vertical axis). A measurement sequence (4 sec duration) consists in moving H across the subject's pupil along five horizontal lines 1 mm apart. The radiant flux Φ_m is measured as a function of the co-ordinates x and y of H.

From the above consideration, we propose that the position of H at which the flux Φ_m is maximal corresponds to the *average* pupil intercept of the ensemble of

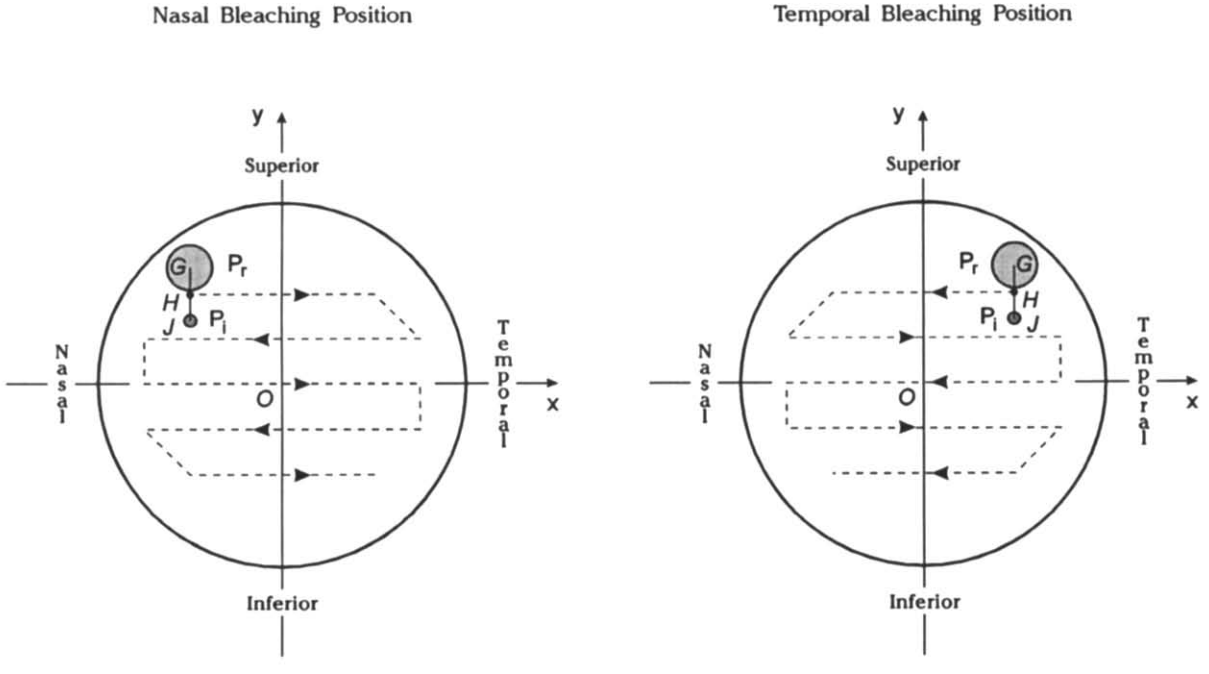

FIGURE 2. *Bleaching position.* The entrance pupil P_i (centre J) and the exit pupil P_r (centre G) are moved jointly inside the subject's pupil. The point H (co-ordinates x, y), the midpoint between J and G, scans the subject's pupil along five horizontal lines 1 mm apart. The abscissa x varies from -3 to $+3$ mm for the three central horizontal lines, but only from -2 to $+2$ mm for the two others. The green beam is left stationary at the start of the pupil scan for a period of 10 sec. The motors are then actuated and the pupil is scanned in 4 sec.

photoreceptors' axes within the sample field R_f'. It should be noted that light guided in the outer segments is more attenuated by the photopigment than unguided light, as demonstrated by van Blokland and van Norren (1986). Therefore, highest accuracy will be attained under strong bleached conditions. To this purpose the lightbeam was left stationary at the start of the pupil scan (Fig. 2) for a period of 10 sec. Then the pupil was scanned in 4 sec. We could choose either of the two bleaching positions depicted in Fig. 2.

In order to assess the possible non-photoreceptor contributions, we used two different pupillary configurations, depicted in Fig. 3. Unless otherwise specified, measurements are carried out with nasal bleaching position and vertical pupils.

Photoreceptor alignment reflectometer

An optical diagram of the PAR is given in Fig. 4. Fixation is provided by a red 633 nm He–Ne laser (Edmund Scientific), yielding a retinal irradiance of 0.9 mW/cm^2 which is safe for 8 hr (ANSI 136.3, 1988). The measuring beam is provided by an unpolarized green 543 nm He–Ne laser (Melles Griot), yielding a retinal irradiance of 0.8 mW/cm^2 (safe time of 10 min). The retinal irradiance E was calculated assuming for the eye a transmittance of 1.0 and a posterior focal length of 22.28 mm ($E = \Phi_{cor}/s$, where s is the illuminated retinal area and Φ_{cor} is the radiant flux incident on the cornea). The fixation beam is combined with the measuring beam (dark grey) through beam splitter T_1, and both beams are directed towards the eye by reflection on beam splitter T_2. Light reflected from the fundus (light grey) is transmitted by beam splitter T_2, then collected by the optical system with accurate control of both the pupillary and retinal focus. The radiant flux is measured by the photomultiplier PMT (Hamamatsu R 647-01); this detector type was chosen because of its high anode sensitivity and low anode dark current.

The spatial filters [L_1, $\mathscr{P}_f$] and [L_4, $\mathscr{P}_i$] remove spatial noise from the laser beams and expand them. The circular diaphragms $\mathscr{P}_i$ and $\mathscr{P}_r$ are conjugate with the entrance pupil P_i and the exit pupil P_r respectively. We chose a green He–Ne laser for measurements because of its radiance (such that the entrance pupil P_i be small) and its wavelength (such that the contribution of light reflected by the sclera and the choroid to the radiant flux Φ_m be low).

The circular diaphragms $\mathscr{R}_i$ and $\mathscr{R}_r$ are focussed on the retina. The diaphragm $\mathscr{R}_r$ defines the retinal area (R_r' in Fig. 1) from which light is collected by the PMT; four sample field diameters are available (1, 2, 3 and 4 deg). The diaphragm $\mathscr{R}_i$ defines the retinal area (R_i') which is illuminated by the green light. The diameter of R_i' is adjusted to be 1 deg larger than that of R_r' to insure that R_r' is always within the bleached area R_i' despite spherical aberrations and eye movements.

The diaphragm $\mathscr{R}_f$ defines the fixation target (5 min arc in diameter). The operator selects the retinal eccentricity (0–8 deg, in any direction) by rotating mirror M_1. Since M_1 is conjugate with the subject's pupil, this does not change the position of P_f in the subject's pupil.

The objectives L_5 and L_{12} are mounted on a plate which is moved transversally in steps of 10 μm by the stepping motors X and Y (Klinger Scientific Corp.). This allows the entrance pupil (P_i) and exit one (P_r) to scan the subject's pupil according to the paths depicted in Fig. 2. We have chosen a Cartesian pattern rather than a circular pattern (more suited to the shape of the subject's pupil) because photoreceptors can be oriented to any point of the pupil plane Oxy. We have limited the

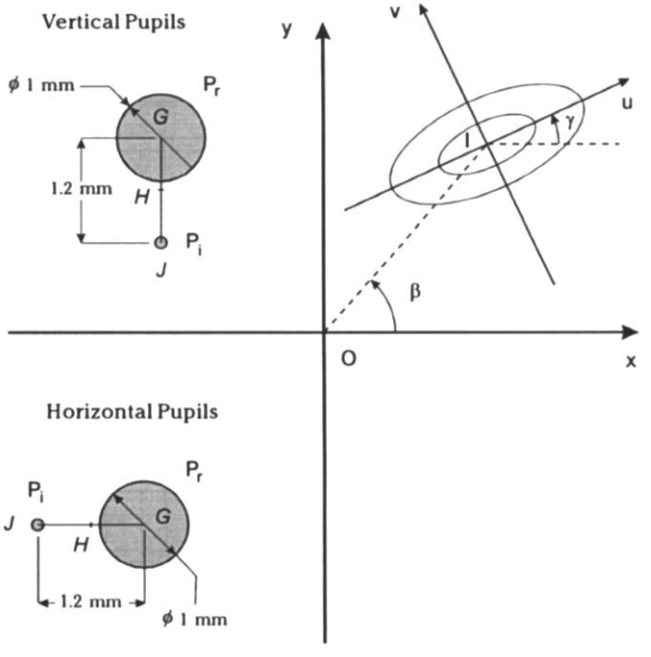

FIGURE 3. *Pupillary configuration.* Vertical pupils: G (centre of the exit pupil) is 1.2 mm above J (centre of the entrance pupil). Horizontal pupils: G is 1.2 mm at the right of J. Isoflux curves are ellipses centred around I. Iu is the focal axis of these ellipses, Iv the axis perpendicular to Iu.

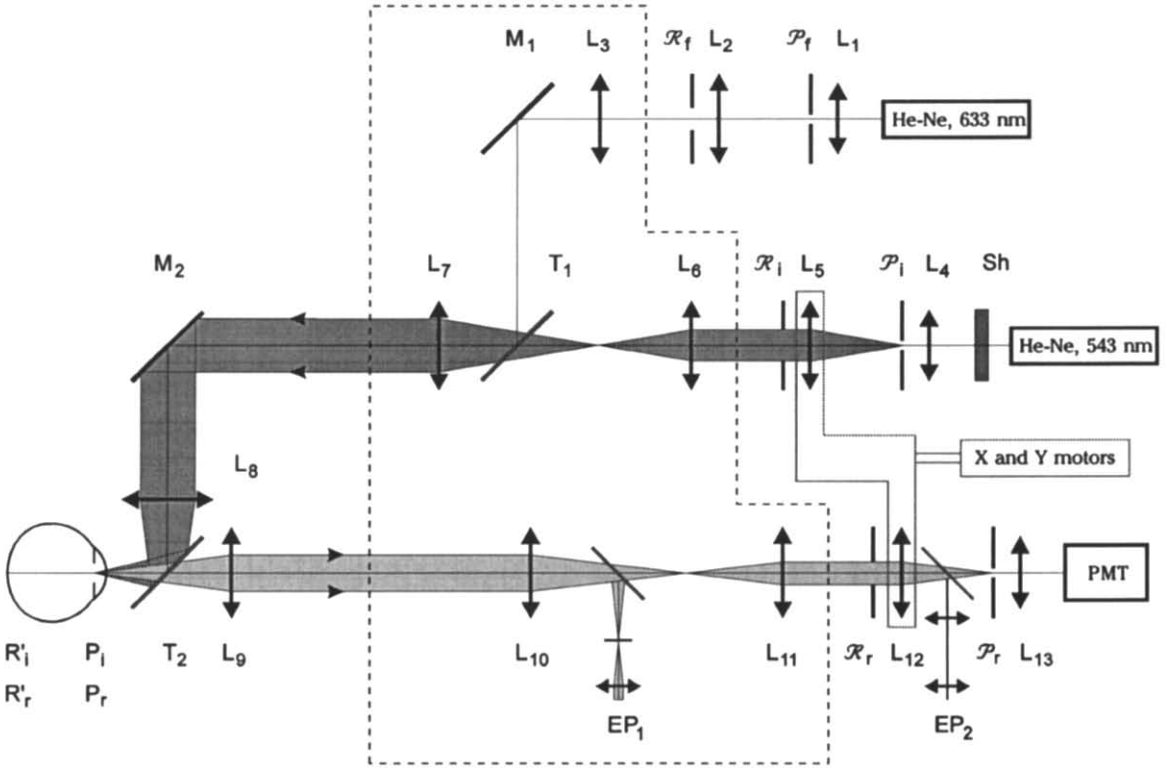

FIGURE 4. *Optics of the instrument.* The fixation beam (red He–Ne laser) is combined with the measuring beam (green He–Ne laser) through dichroic beam splitter T_1. The reflected light (light grey) is separated from the incident light (dark grey) by beam splitter T_2. PMT: photomultiplier. $\mathscr{P}_f$, $\mathscr{P}_i$ and $\mathscr{P}_r$: circular diaphragms conjugate to the subject's pupil. $\mathscr{R}_f$, $\mathscr{R}_i$ and $\mathscr{R}_r$: circular diaphragms conjugate to the retina. M_1 and M_2: mirrors. L_1–L_{13}: objectives, EP_1 and EP_2: eyepieces.

number of scanned horizontal lines to 5 (1 mm apart) so that the measurement duration be only 4 sec.

The head of the subject is stabilized by a bite bar which is fixed on a three-dimensional positioner. The operator uses an eyepiece EP_1 (reticule: concentric circles) for centring and focus of the subject's pupil.

The components L_3, L_6, L_7, L_{10}, L_{11}, M_1 and T_1 are mounted on a single plate (dotted lines in Fig. 4) which can be shifted longitudinally, thus allowing focus adjustment from -12 to $+12$ D of ametropia. The operator uses a second eyepiece EP_2 to focus the retina.

An IBM compatible computer controls the shutter Sh (green light), the two stepping motors (via an IEEE 488 interface), and receives input from the PMT. The electric signal collected by the PMT is sampled at every horizontal step (7.14 μm in the plane of the subject's pupil), converted into a digital signal (10 bits), then stored in the computer memory. Fifty-six successive samples are averaged ($56 \times 7.14\,\mu m = 400\,\mu m$). A map of the measured flux is created by the computer (an example is given in Table 1) within seconds after data acquisition, allowing immediate inspection of the data.

Series of measurements with a model eye were carried out to indicate the magnitude of the angular dependence of the radiant flux Φ_m in case of a diffuse reflector. With a barium sulphate surface as "fundus" ($96 \pm 3\%$ reflectance), the radiant flux Φ_m through the exit pupil P_r does not vary more than $\pm 5\%$ for the different positions (x, y) in the pupil.

Data analysis

The experimental data consisted of the radiant flux values Φ_m at different positions (x, y) in the pupil (Table 1). To describe our data we chose a function Φ

TABLE 1. Illustrative data Φ_m from a single scan (subject S2)

								x							
y	−2.8	−2.4	−2.0	−1.6	−1.2	−0.8	−0.4	0.0	0.4	0.8	1.2	1.6	2.0	2.4	2.8
2					153	157	159	156	151	138	129				
1		185	221	273	304	339	333	293	252	210	172	186	181	143	
0	208	256	333	464	567	624	603	518	415	316	242	189	161	144	141
−1	200	267	358	512	643	721	688	554	429	324	243	194	165	144	130
−2				277	327	341	342	309	252	203	164	143			

x and *y* are the distances from H to the centre of the pupil (in mm).

which is the sum of a constant and a Gaussian function:

$$\Phi(x, y) = A + B\ 10^{-[\zeta_x (x-x_0)^2 + \zeta_c (x-x_0)(y-y_0) + \zeta_y (y-y_0)^2]}. \quad (1)$$

The Gaussian function was taken on the analogy of the equation proposed by Stiles (1937) to represent the Stiles–Crawford function.

The co-ordinates x_0 and y_0 give the position of H in the subject's pupil corresponding to the maximum flux (positive xs, temporal; positive ys, superior). We denote β (Fig. 3) the angle (Ox, OI), where I is the point of co-ordinates (x_0, y_0).

The total flux at (x_0, y_0) is the sum of a diffuse component A and a directional component B. The ratio B/A, ratio of directional to diffuse flux when H is at (x_0, y_0), depends on the relative quantity of guided light.

Isoflux curves are ellipses centred around I. Let Iu be the focal axis of these ellipses, and Iv be the axis perpendicular to Iu. In the co-ordinate system Iuv, function Φ becomes:

$$\Phi(u, v) = A + B\ 10^{-[\zeta_u u^2 + \zeta_v v^2]}. \quad (2)$$

The directionality factors ζ_u and ζ_v describe the sharpness of $\Phi(u, v)$ along directions Iu and Iv respectively; the higher ζ_u and ζ_v values, the steeper function Φ. We chose the orientation of Iu such that the angle γ between Ox and Iu be in the range]−90 deg 90 deg] (Fig. 3).

We characterize photoreceptor directionality by the three parameters γ, ζ and e. The angle γ between the horizontal and focal axes is:

$$\gamma = \gamma_0 \quad \text{if } \zeta_x < \zeta_y, \quad \text{where} \quad \gamma_0 = \tfrac{1}{2} \arctan \frac{\zeta_c}{\zeta_x - \zeta_y}$$

$$\gamma = \gamma_0 - 90^\circ \quad \text{if} \quad \zeta_x > \zeta_y \text{ and } \zeta_c > 0,$$

$$\gamma = \gamma_0 + 90^\circ \quad \text{if} \quad \zeta_x > \zeta_y \text{ and } \zeta_c \leqslant 0. \quad (3)$$

The mean directionality factor ζ is:

$$\zeta = \frac{\zeta_u + \zeta_v}{2} = \frac{\zeta_x + \zeta_y}{2}. \quad (4)$$

The eccentricity e of isoflux ellipses is:

$$e = \sqrt{\frac{\zeta_v - \zeta_u}{\zeta_v}} = \sqrt{\frac{(\zeta_y - \zeta_x)\cos 2\gamma - \zeta_c \sin 2\gamma}{\zeta_x \sin^2\gamma - \zeta_c \cos\gamma \sin\gamma + \zeta_y \cos^2\gamma}}. \quad (5)$$

Experimental data further than 3 mm from the peak were rejected because Safir and Hyams (1969) showed that the Gaussian fits were inappropried at such high distances. Weighted least-squares fits to the remaining data were used to determine the seven unknown parameters x_0, y_0, A, B, ζ_x, ζ_c and ζ_y. Data were weighted on the analogy of Stiles–Crawford effect studies, where the density of collected data generally does not depend on the distance from the peak (since Stiles–Crawford functions are measured along a single axis, commonly the horizontal diameter Ox). We divided the plane Oxy into six circular rings (labelled from $i = 1$ to $i = 6$) centred on the peak and whose inner and outer diameters were $(i - 1) \times 0.5$ mm and $i \times 0.5$ mm respectively. We gave the weight $1/n_i$ to data inside ring i, where n_i was the number of data inside ring i.

Maps of isoflux contours were created by interpolating between measured values and assigning different greys to ranges of flux values. Interpolation between measured values (Table 1) was performed with the function $10^{-[\zeta_x (x-x_0)^2 + \zeta_c (x-x_0)(y-y_0) + \zeta_y (y-y_0)^2]}$, where the parameters x_0, y_0, ζ_x, ζ_c and ζ_y have the above determined values.

Subjects and procedure

The study population was 20 normal subjects in good health and free of ocular pathology (15 males, 5 females; 11 OD, 9OS). Visual acuity in all cases was correctable to 20/20 or better. The ages of the subjects ranged from 20 to 60 yr (with five subjects in each decade). The subjects S1 (29 yr), S2 (34 yr), S3 (33 yr) and S4 (32 yr) participated in experiments designed to study the contribution of possible spurious effects.

After giving informed consent to the protocol approved by an Institutional Review Board, the subject was tested in one experimental session. The pupil was dilated by application of 1% Mydriacyl to a minimum of 7 mm dia. The subject's eye was then aligned to the PAR. With the subject looking at the fixation spot ($\mathscr{R}_f$), the subject's pupil was brought into focus and centred by using the retractable eyepiece EP_1 (Fig. 4). The retractable eyepiece EP_2 was then used to bring into focus the retina, which was lighted by the attenuated green spot (retinal irradiance of 0.08 mW/cm^2 for less than 20 sec).

Shutter Sh was opened and the green beam left stationary at the start of the pupil scan (Fig. 2) for a period of 10 sec (retinal irradiance of 0.8 mW/cm^2). This allowed for the bleaching of more than 95% of the photopigment (Rushton & Henry, 1968). The motors X and Y were then actuated, and the pupil scanned in 4 sec.

In this study, we used a test field of 2° in dia (580 μm on the retina). The measurement was repeated three times for each experimental condition. The centring of the pupil of the subject was checked and readjusted if necessary before each measurement.

Non-photoreceptor contributions

We have compared the photoreceptor orientation (x_0, y_0), directionality ζ and ratio B/A for different pupillary configurations, bleaching positions and retinal eccentricities. Only four subjects underwent this set of measurements, whose purpose was to assess whether instrumental bias, bleaching position, and specular reflection by the inner limiting membrane introduce any systematic errors in the measurement of photoreceptor orientation with the PAR method.

We have not carried out measurements without bleaching of the photopigment, since the signal-to-noise ratio was not high enough to measure Φ_m in such conditions; thus interpretation of our results may be subject to artefactual reflections. We have not taken account of the finite size of the entrance and exit pupils, nor of the data accumulation into 0.4 mm blocks in the x direction: we prepare a paper where a model of fundus reflection allows us to determine their effects.

RESULTS

Maps of isoflux contours for the 20 subjects are presented in Fig. 5. The grey gives the relative radiant power in percent, i.e. $100\,\Phi(x, y)/(A + B)$. The test field (dia 580 μm) was centred on the foveola. Each of these 20 maps corresponds to only one measurement.

Photoreceptor orientation

Figure 6 gives the co-ordinates x_0 and y_0 for the 20 subjects. Each point represents the average of three measurements (SD < 0.2 mm). The mean horizontal peak location is 0.86 mm nasal (SD = 0.84 mm), and the mean vertical peak location is 0.09 mm inferior (SD = 0.73 mm). The results for most subjects are clustered within a 4 mm dia circle around the centre of the pupil. However three subjects have photoreceptors with a pronounced tilt: two in the nasal direction and one in the inferior direction.

OI was defined as the distance from the centre of the subject's pupil to the point of co-ordinates (x_0, y_0). The mean value of OI is 1.22 mm (SD = 0.69 mm). No correlation was found between OI and age ($r = -0.127$, $P = 0.59$).

Photoreceptor directionality

Directionality properties are characterized by the directionality factor ζ, the eccentricity e and the angle γ between the horizontal and focal axes. Figure 7 shows these parameters as a function of age. The mean

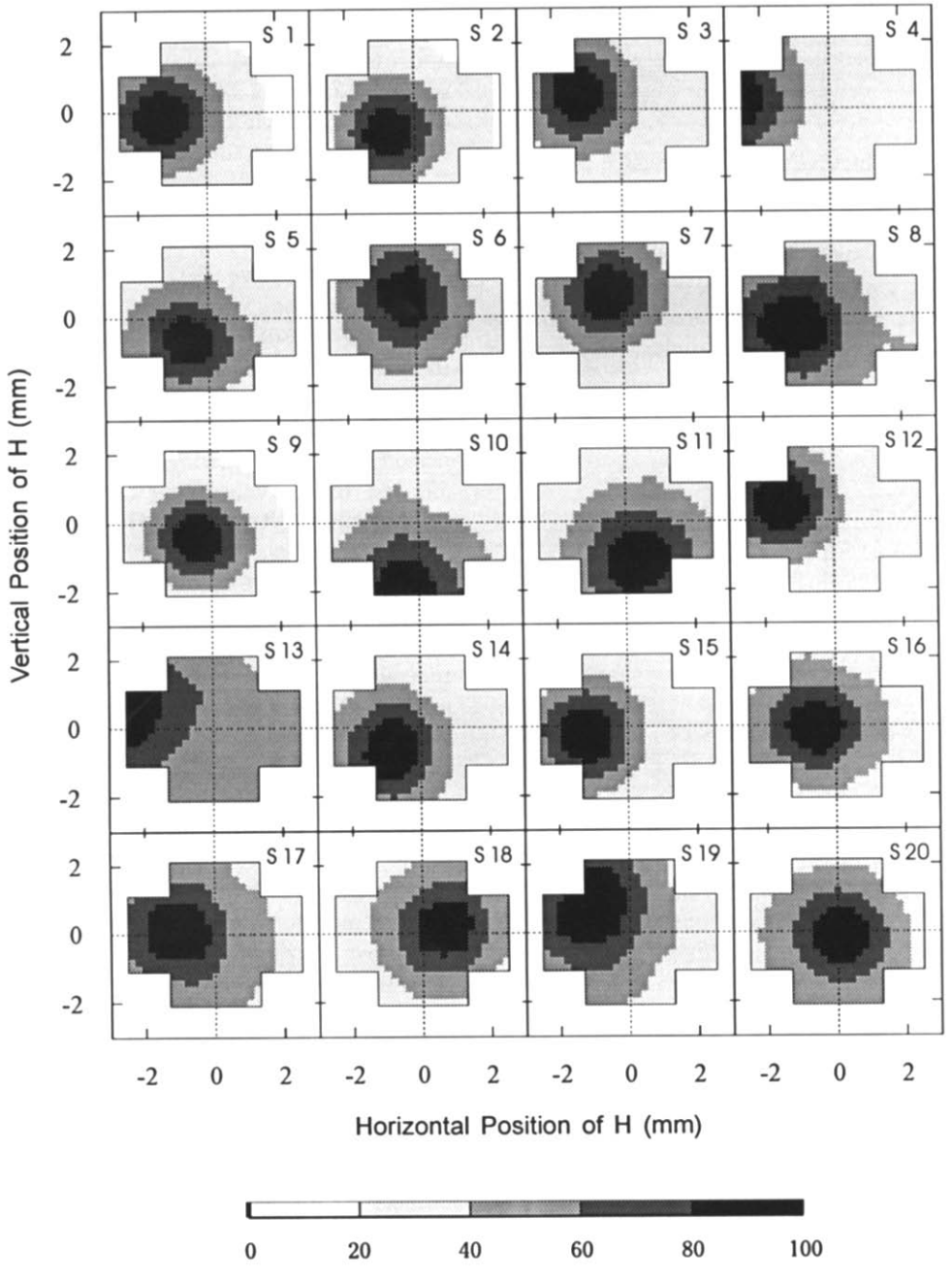

FIGURE 5. *Maps of isoflux contours.* The grey gives the relative radiant power in percent, i.e. $100\,\Phi(x, y)/(A + B)$. The sample field (dia 580 μm) was centred on the foveola. Each of these 20 maps corresponds to only one measurement.

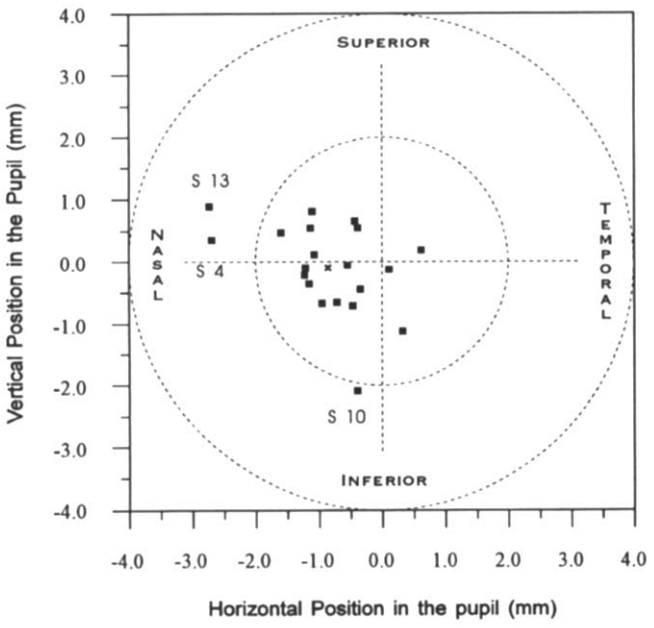

FIGURE 6. Orientation of foveolar photoreceptors (20 subjects). Each point is the average of three measurements. The diameters of the two dotted circles are 4.0 and 8.0 mm.

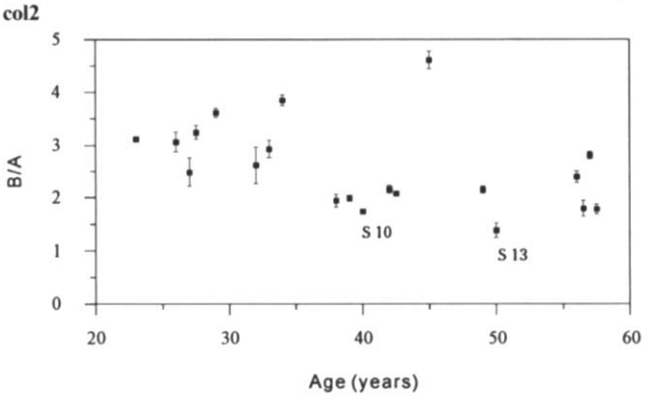

FIGURE 8. Ratio B/A of directional to diffuse flux as a function of age (20 subjects). Each point is the average of three measurements. The bars represent ± 1 SD of the mean.

values and SDs of ζ_x, ζ_c, ζ_y, ζ_u, ζ_v, ζ, e and γ are given in Table 2. The factor ζ_x correlates with ζ_y ($r = 0.849$, $P < 0.0001$).

The directionality factor ζ does not vary significantly with age ($r = -0.136$, $P = 0.57$), but decreases with OI ($r = -0.604$, $P = 0.005$).

In Fig. 7, we have plotted values of angles γ and β (see Fig. 3) for the seven subjects whose eccentricity e is significantly larger than 0.3 ($P < 0.05$).

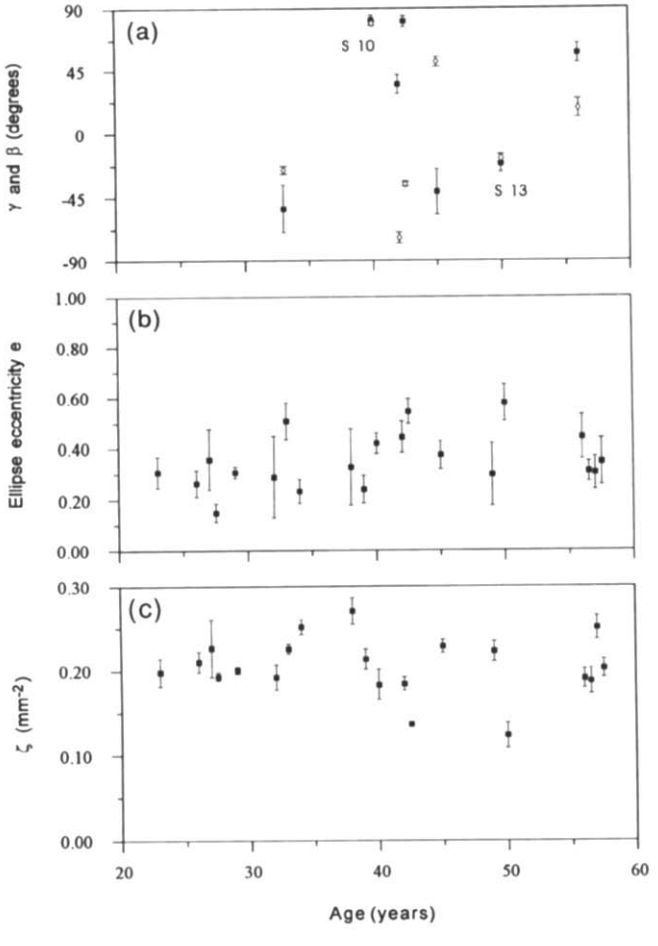

FIGURE 7. (a) ■: angle γ between the horizontal and focal axes. ◇: angle β between Ox and OI (seven subjects). (b) Eccentricity e of isoflux ellipses (20 subjects). (c) Directionality factor ζ as a function of age (20 subjects). Each point is the average of three measurements. The bars represent ± 1 SD of the mean.

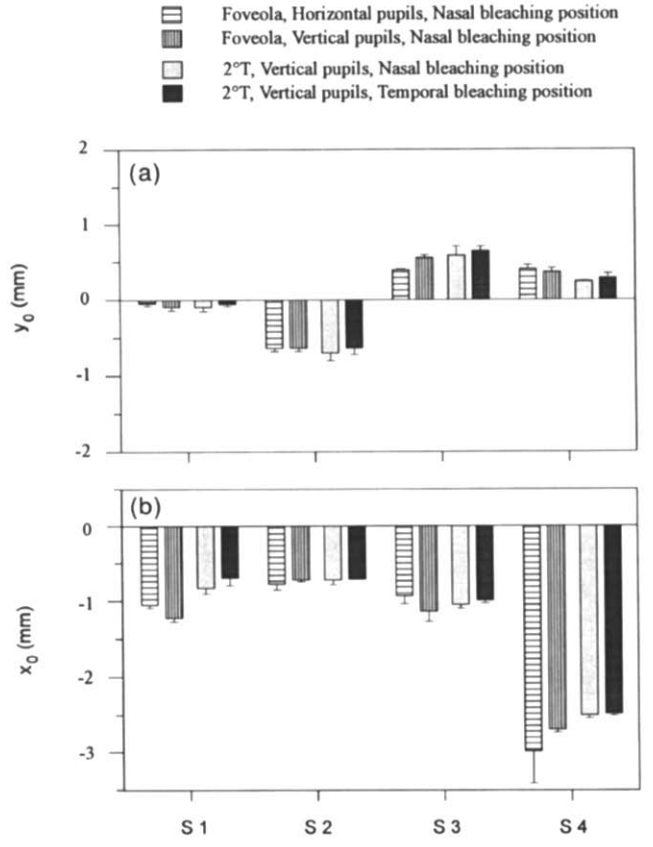

FIGURE 9. Values of x_0 and y_0 for two retinal eccentricities (0° and 2°T), two bleaching positions (nasal and temporal) and two pupillary configurations (horizontal and vertical pupils). Means of three measurements $\pm$ SD.

TABLE 2. Mean values and SDs of the directionality factors, the eccentricity e and the angle γ (20 subjects)

	ζ_x (mm^{-2})	ζ_c (mm^{-2})	ζ_y (mm^{-2})	ζ_u (mm^{-2})	ζ_v (mm^{-2})	ζ (mm^{-2})	e	γ (deg)
Mean	0.205	0.003	0.203	0.189	0.219	0.204	0.352	−3.91
SD	0.034	0.023	0.039	0.038	0.034	0.035	0.109	44.43

Ratio of directional to diffuse flux

The ratio B/A is on average 2.59 (SD = 0.82). Figure 8 gives the ratio B/A as a function of age: the ratio B/A shows a tendency to decrease with age ($r = -0.436$, $P = 0.05$). The ratio B/A does not correlate with OI ($r = -0.258$, $P = 0.27$). It increases with ζ_u ($r = 0.451$, $P = 0.05$), but shows no significant correlation with ζ ($r = 0.424$, $P = 0.06$) or ζ_v ($r = 0.382$, $P = 0.10$).

Pupillary configuration, bleaching position and retinal eccentricity

We carefully examined the values of orientation, directionality and ratio of directional to diffuse flux for different pupillary configurations, bleaching positions and retinal eccentricities. Figure 9 gives the values of x_0 and y_0 for two retinal eccentricities (0° and 2°T), two bleaching positions (nasal and temporal) and two pupillary configurations (horizontal and vertical pupils). Figure 10 gives the values of ζ and B/A for the two same retinal eccentricities (with nasal bleaching position and vertical pupils).

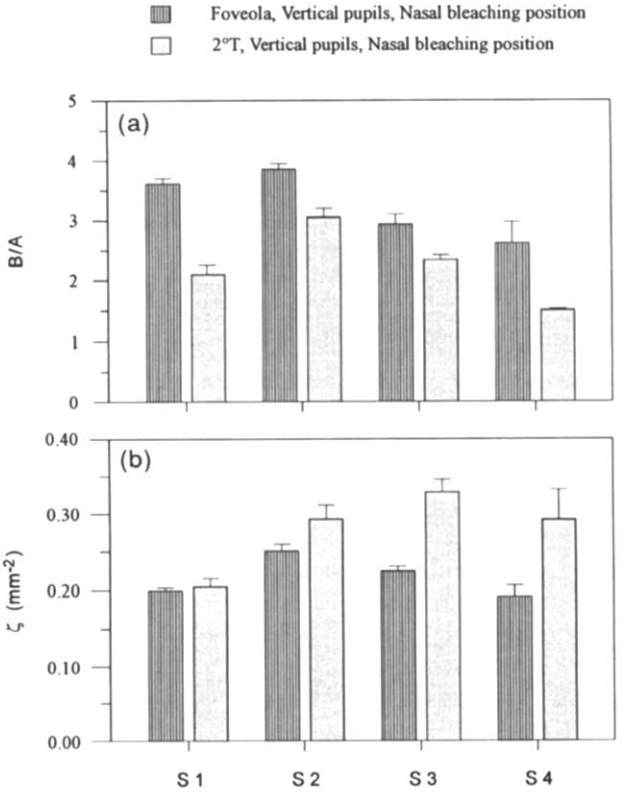

FIGURE 10. Values of ζ and B/A in the foveola and at 2°T (with nasal bleaching position and vertical pupils). Means of three measurements ± SD.

DISCUSSION

It is critical to assess whether instrumental bias, bleaching position, and specular reflection by the inner limiting membrane introduce any systematic errors in the measurement of photoreceptor orientation with the PAR method.

Instrumental bias

The pupillary configuration denoted *vertical pupils* is symmetric around a vertical line (Fig. 3). The horizontal component of the photoreceptor mean orientation, x_0, is clearly defined since G, H, and J have identical x-values. On the other hand the meaning of y_0 is unclear since the diameters of the two pupils are different and the y-values of G, H, and J are not equal. Clear definition of y_0 requires a pupillary configuration where the line JG is horizontal. The values of x_0 and y_0 determined at the foveola with *horizontal pupils* are not significantly different from those measured with *vertical pupils* (Fig. 9, left bars), except in two cases (for S1, whose values of x_0 have a difference of 0.17 mm; for S3, whose values of y_0 have a difference of 0.16 mm). Nevertheless these differences of 0.17 and 0.16 mm are small. Thus, the use of a single pupillary configuration is sufficient to provide accurate measures of the horizontal *and* vertical components of the photoreceptor orientation.

Bleaching conditions

MacLeod (1974) developed a selective adaptation technique to study the variability of photoreceptor orientations: an adapting light which traversed the subject's pupil at J affected the subgroup of photoreceptors oriented towards J more efficiently than the subgroups oriented towards other points; so this subgroup was less sensitive to the test light than the others. The PAR procedure presents an analogy with this experience; for *nasal bleaching position* each measurement is preceded by a 10 sec bleaching period, with J located at $\{x_J = 2$ mm nasal, $y_J = 1.4$ mm superior$\}$. To investigate whether the position of the maximum depends on the direction of the bleaching light onto the photoreceptors, we chose another location of J during the bleaching period (Fig. 2, *temporal bleaching position*). Results in Fig. 9 (right bars) show that the values of x_0 and y_0 are not significantly different for the two bleaching positions. Therefore the position of the peak does not depend on the location of J in the subject's pupil for a 95% bleach.

Specular reflection by the inner limiting membrane

A significant contribution of the specular reflection by the inner limiting membrane (ILM) would yield a

maximum in $\Phi(x, y)$ corresponding to the orientation of the normal to the ILM. Since the slope of the foveal pit varies rapidly with eccentricities (Gorrand, Delori & Snodderly, 1989), one would expect marked changes in the position of this maximum with retinal eccentricities. Figure 9 (middle bars) gives photoreceptor orientation (x_0, y_0) for the four subjects measured at two retinal eccentricities (0° and 2° temporal). The results for subjects S2, S3 and S4 show close positions of the maxima in $\Phi(x, y)$, indicating that the ILM contributions are small compared to the radiant flux guided backwards by photoreceptors. The case of subject S1 will be discussed later.

Comparison with psychophysics

In psychophysics the directionality is characterized by the shape factors ρ_x and ρ_y, derived from the relative luminous sensitivity (Stiles, 1937):

$$\eta = 10^{-\rho_x (x - x_0)^2} \text{ (horizontal pupil traverse)},$$
$$\eta = 10^{-\rho_y (y - y_0)^2} \text{ (vertical pupil traverse)}, \quad (6)$$

where x_0 and y_0 are the co-ordinates for the maximum of the Stiles–Crawford function.

Wijngaard and Kruysbergen (1975) pointed out that non-guided light which is absorbed by photopigment is approximately independent of the angle of incidence. Therefore the sensitivity η of a cone should reach a constant level when this angle is large enough to make the guided light negligible. Equation (6) does not include a constant, so it cannot be used to fit data far from the peak.

Applegate and Lakshminarayanan (1993) formed a normative data base for the normal variation of photoreceptor alignment, as determined by the Stiles–Crawford function. Their data base included 53 eyes with horizontal pupil traverses, and 49 eyes with vertical ones. The mean horizontal peak location was 0.51 mm nasal (SD = 0.72 mm), the mean vertical peak location 0.20 mm superior (SD = 0.64 mm). These values are on the same order as those obtained with the PAR. Both methods demonstrate a tendency for photoreceptors to be oriented towards the nasal side of the pupil. Since the fovea is on the temporal side of the eye optical axis, it is commonly assumed that this nasal shift of the SC peak favours rays whose angles of incidence upon the cornea are low, i.e. rays with small aberrations (this nasal shift would be 0.42 mm if the angle α between the optic and visual axes was 5°).

The data base of Applegate and Lakshminarayanan (1993) also gives the shape factors ρ_x and ρ_y. In the fovea the mean value of ρ_x was 0.047 mm^{-2} (SD = 0.013 mm^{-2}) and the mean value of ρ_y 0.053 mm^{-2} (SD = 0.012 mm^{-2}). The mean value of ζ (0.204 ± 0.035 mm^{-2}) measured in the foveola with the PAR is thus 4.1 times the value of ρ measured by psychophysics. Nevertheless it should be noted that the transient Stiles–Crawford effect gives results closer to reflectometry: utilizing the criterium of critical flicker frequency, Bailey and Heath (1978) measured directional sensitivity functions much narrower than standard Stiles–Crawford functions (i.e. shape factors much higher).

van Blokland (1986) assessed the alignment characteristics of the foveolar cones by measuring the radiant flux distribution along an horizontal line through the centre of the subject's pupil. He derived an "absorbance diagram" by subtracting the distribution obtained in the unbleached state from that obtained in bleached condition. He found that the shape factor ζ of this diagram was 2 times (instead of 4.1) the shape factor ρ of the Stiles–Crawford function. But van Blokland's measurements were done with a fixed entrance pupil. In contrast, the entrance and exit pupils of the PAR jointly scan the entire subject's pupil, which provides a better two-dimensional determination of the photoreceptor orientation. Furthermore, a single measurement sequence is enough with the PAR to determine the orientation of tilted cones (such as in subject S4) whereas successive measurements with different entrance pupils are needed in van Blokland's technique. Finally, the PAR provides a more sensitive measurement of the directionality (higher values of ζ) than van Blokland's method, because it combines a variation of both the collection angle as well as the incidence angle.

Misalignment of photoreceptors

The directionality depends on the acceptance angle of individual photoreceptors and on the variability of their orientation within the tested photoreceptor population. Safir and Hyams (1969) suggested that the acceptance angles of individual cones were narrow, and that the Stiles–Crawford effect was mainly due to the splaying of cones. On the other hand MacLeod (1974) concluded from his experiments that the foveal cones were aligned with great precision.

The directionality factor ζ decreases with OI ($r = -0.604$, $P = 0.005$), i.e. when photoreceptors are tilted. A lower directionality follows either from larger acceptance angles of photoreceptors, either from higher variability of photoreceptor orientations within the sample field. The second hypothesis seems plausible since tilted photoreceptors can be non-uniformly tilted.

By definition of the co-ordinate system Iuv, photoreceptors within the sample field are more stretched along the focal axis Iu than along the axis Iv. Among the seven subjects whose eccentricity e was significantly larger than 0.3, two had also very eccentric peaks (S10 and S13): interestingly their angles β and γ are very close one to another (Fig. 7), which means that their photoreceptors are stretched radially. Subject S4 also had a pronounced tilt (Fig. 6), but its eccentricity e was lower than 0.3.

In case of misalignment, patterns radiated by photoreceptors to the subject's pupil are no more superimposed and B/A decreases. Since photoreceptors are stretched along the focal axis Iu, we can guess that radiated patterns be better superimposed along the direction Iv than along the direction Iu. Effectively B/A correlates much more with ζ_u ($r = 0.451$, $P = 0.046$) than with ζ_v ($r = 0.382$, $P = 0.097$).

Effect of age

The ratio B/A of directional to diffuse flux shows a tendency to decrease with age ($r = -0.436$, $P = 0.05$). The ratio B/A depends on the photoreceptor coverage and on the structure of the pigment epithelium (PE). Curcio, Millican, Allen and Kalina (1993) counted cones and rods in central retinas from 27 donors aged 27–90 yr, and found that the photoreceptor coverage was similar at all ages. Feeney-Burns, Berman and Rothman (1984) observed changes in PE cell structure with age. Thus the decrease of B/A is probably due to these PE changes.

Effect of retinal eccentricity

The directionality factor ζ is larger at 2°T than in the foveola (except for subject S1, Fig. 10). This result agrees with psychophysical measurements: Enoch and Hope (1973) found that the shape factors of the Stiles–Crawford function were higher at a retinal eccentricity of 2° than in the foveola. This phenomenon could be due to the diameter of the cone myoid, which increases from the foveal centre to the foveal edge.

For subject S1 the directionality factor ζ at 2°T is relatively small. This is probably linked to the above observation that the values of x_0 at 2°T and in the foveola are different one from another (Fig. 9), which stretches photoreceptors.

Finally the ratio B/A is much lower at 2°T than in the foveola (Fig. 10).

Physical parameters affecting the photoreceptor directionality

The different absorbers and reflectors of the ocular fundus were investigated by van Norren and Tiemeijer (1986) and Delori and Pflibsen (1989). The contribution of light reflected by the sclera and the choroid to the aerial image is low at 543 nm because of the high absorption of blood. The foveal cones are quite different from those outside the fovea; their outer segments are twice as long and closely crowded together. Under normal path illumination, Enoch (1961) could observe modal patterns inside the outer segment (OS), and thereby demonstrate the waveguide behaviour of photoreceptors.

The number of modes that are guided through a waveguide depends on the waveguide parameter V defined by (Snitzer, 1961):

$$V = \frac{\pi\phi}{\lambda}\sqrt{n_{co}^2 - n^2}$$

where λ is the wavelength in vacuum, ϕ the waveguide diameter, and n_{co} and n the refractive indices of the core and surrounding medium, respectively (Fig. 11). Using values available in the literature we find $V = 2.93$ and 2.58 for the myoid and OS, respectively. Only the modes HE_{11} (two modes) and LP_{11} (four modes) have cut-off values < 2.58, and therefore are capable of propagating along the myoid *and* the OS. It should be noted that tapered ellipsoid waveguide could cause coupling among modes. However Snyder (1970) showed that there is no coupling among bound modes for $V < 3.832$.

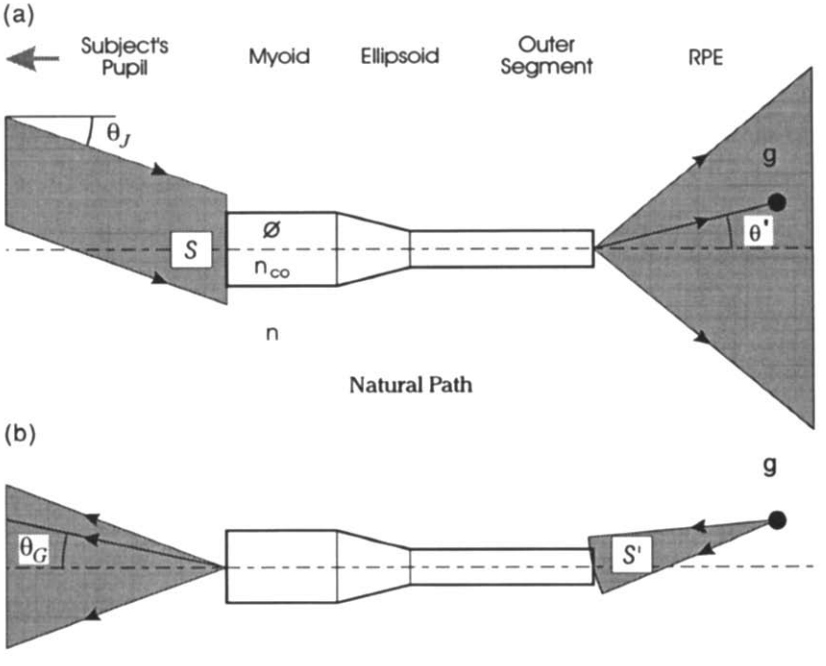

FIGURE 11. *Model of photoreceptor.* (a) The wave coming from J launches the bound modes. Light is guided along the photoreceptor, and radiated into the RP. (b) The wave backscattered by the granule g launches the bound modes. Light is guided backwards, and radiated to the subject's pupil.

More rigorous analysis of our results will be presented in a paper in preparation. The intuitive arguments which follow assume that the photopigment is bleached, and that all photoreceptors inside the test field are aligned to the same pupillary point I. Figure 11a shows a wave coming from J and falling upon the anterior face of a myoid. When the angle of incidence θ_J upon the myoid is small (J close to I), this wave launches the HE_{11} and LP_{11} modes; light is guided along the myoid, the ellipsoid and the OS, then radiated from the OS tip into the pigment epithelium (PE). But when the angle of incidence θ_J upon the myoid is large (J far from I), the incident wave cannot launch the guided modes: light simply passes through the photoreceptor.

Light emerging from the outer segments spreads into the PE. The scleral ends of the foveal cone OSs are embedded in the PE, unlike cones elsewhere. When θ_J is small, light is guided along the photoreceptors, and the flux density is higher in the vicinity of OS axes. A wavelet backscattered from a granule g located inside the acceptance angle of an OS is likely to launch the HE_{11} and LP_{11} modes backwards (Fig. 11b). On the other hand when θ_J is large, the flux density inside the PE is homogeneous; wavelets backscattered from granules whose colatitudes θ' are large cannot launch the guided modes. To summarize, the radiant power falling upon the PE is constant, whatever θ_J may be, but the flux density inside the PE depends on θ_J. Consequently the radiant power carried backwards by modes guided along photoreceptors is much higher for $\theta_J = 0$ (i.e. when light enters the pupil along photoreceptor axes), than for large values of θ_J (J far from I).

Light guided backwards along the photoreceptor is then radiated from the myoid anterior face to the subject's pupil. The radiant power collected through the exit pupil is maximal when its centre G is close to I, and decreases when the distance GI increases.

The entrance and exit pupils of the PAR jointly scan the entire subject's pupil. So the radiant power collected through the exit pupil is much more when J and G are close to I than when they are far from I. The directionality factor measured by reflectometry is higher than the shape factor provided by psychophysics, where only the position of J has to be taken into account.

Conclusions

In conclusion, the photoreceptor alignment reflectometer appears to offer a useful tool to study photoreceptor alignment in clinical situations because of its high sensitivity, its flexibility, the ease of use for subjects and the rapidity with which measurements are performed. Measurements are possible as far as 8° from the fovea. Joint electromechanical scanning of the entrance and exit pupils provides both rapidity of data acquisition and high sensitivity for the determination of the photoreceptor orientation. Finally, the technique is not significantly influenced by reflections from the limiting membrane and the anterior media, and appears unaffected by changes in pupil configuration and bleaching conditions.

REFERENCES

American National Standards Institute (ANSI) (1988). *Safe use of lasers*, Z-136.3. New York: ANSI.

Applegate, R. A. & Lakshminarayanan, V. (1993). Parametric representation of Stiles–Crawford functions: Normal variation of peak location and directionality. *Journal of the Optical Society of America A, 10*, 1611–1623.

Bailey, J. E. & Heath, G. G. (1978). Flicker effects on receptor directional sensitivity. *American Journal of Optometry and Physiological Optics, 55*, 807–812.

Bailey, J. E., Lakshminarayanan, V. & Enoch, J. M. (1991). The Stiles–Crawford function in an aphakic subject with retinitis pigmentosa. *Clinical Vision Sciences, 6*, 165–170.

Bedell, H. E. & Enoch, J. M. (1979). A study of the Stiles–Crawford (S–C) function at 35° in the temporal field and the stability of the foveal S–C function peak over time. *Journal of the Optical Society of America, 69*, 435–442.

Birch, D. G., Sandberg, M. A. & Berson, E. L. (1982). The Stiles–Crawford effect in retinitis pigmentosa. *Investigative Ophthalmology and Visual Science, 22*, 157–164.

van Blokland, G. J. (1986). Directionality and alignment of the foveal receptors, assessed with light scattered from the fundus *in vivo*. *Vision Research, 26*, 495–500.

van Blokland, G. J. & van Norren, D. (1986). Intensity and polarization of light scattered at small angles from the human fovea. *Vision Research, 26*, 485–494.

Campos, E. C., Bedell, H. E., Enoch, J. M. & Fitzgerald, C. R. (1978). Retinal receptive field like properties and Stiles–Crawford effect followed in a patient with traumatic choroidal rupture. *Documenta Ophthalmologica, 45*, 381–395.

Curcio, C. A., Millican, C. L., Allen, K. A. & Kalina, R. E. (1993). Aging of the human photoreceptor mosaic: Evidence for selective vulnerability of rods in central retina. *Investigative Ophthalmology and Visual Science, 34*, 3278–3296.

Delori, F. C. & Pflibsen, K. P. (1989). Spectral reflectance of the human ocular fundus. *Applied Optics, 28*, 1061–1077.

Enoch, J. M. (1961). Visualization of waveguide modes in retinal receptors. *American Journal of Ophthalmology, 51*, 1107–1118.

Enoch, J. M. & Hope, G. M. (1973). Directional sensitivity of the foveal and parafoveal retina. *Investigative Ophthalmology and Visual Science, 12*, 497–503.

Feeney-Burns, L., Berman, E. R. & Rothman, H. (1984). Aging human RP: Morphometric analysis of macular, equatorial, and peripheral cells. *Investigative Ophthalmology and Visual Science, 25*, 195–200.

Fitzgerald, C. R., Enoch, J. M., Campos, E. C. & Bedell, H. E. (1979). Comparison of visual function studies in two cases of senile macular degeneration. *Albrecht von Graefes Archiv., 210*, 79–91.

Gorrand, J. M. (1985). Directional effects of the retina appearing in the aerial image. *Journal of Optics, 16*, 279–287.

Gorrand, J. M. (1989). Reflection characteristics of the human fovea assessed by reflecto-modulometry. *Ophthalmic and Physiological Optics, 9*, 53–60.

Gorrand, J. M. & Delori, F. C. (1990). A method for assessing the photoreceptor directionality. *Investigative Ophthalmology and Visual Science, 31*, 425.

Gorrand, J. M., Delori, F. C. & Snodderly, D. M. (1989). Specular reflection from the fovea. *Investigative Ophthalmology and Visual Science, 30*, 366.

MacLeod, D. I. A. (1974). Directionally selective light adaptation: A visual consequence of receptor disarray? *Vision Research, 14*, 369–378.

van Norren, D. & Tiemeijer, L. F. (1986). Spectral reflectance of the human eye. *Vision Research, 26*, 313–320.

Pokorny, J., Smith, V. C. & Johnston, P. B. (1979). Photoreceptor misalignment accompanying a fibrous scar. *Archives of Ophthalmology, 97*, 867–869.

Rushton, W. A. H. & Henry, G. H. (1968). Bleaching and regeneration of cone pigments in man. *Vision Research, 8*, 617–631.

Safir, A. & Hyams, L. (1969). Distribution of cone orientations as an explanation of the Stiles–Crawford effect. *Journal of the Optical Society of America, 59*, 757–765.

Smith, V. C., Pokorny, J. & Diddie, K. R. (1978). Color matching and Stiles–Crawford effect in central serous choroidopathy. *Modern Problems in Ophthalmology, 19*, 284–295.

Smith, V. C., Pokorny, J. & Diddie, K. R. (1988). Color matching and the Stiles–Crawford effect in observers with early age-related macular changes. *Journal of the Optical Society of America A, 5*, 2113–2121.

Snitzer, E. (1961). Cylindrical dielectric waveguide modes. *Journal of the Optical Society of America, 51*, 491–498.

Snyder, A. W. (1969). Excitation and scattering of modes on a dielectric or optical fiber. *IEEE Transactions, MTT-17*, 1138–1144.

Snyder, A. W. (1970). Coupling of modes on a tapered dielectric cylinder. *IEEE Transactions, MTT-18*, 383–392.

Stiles, W. S. (1937). The luminous efficiency of monochromatic rays entering the eye pupil at different points and a new color effect. *Proceedings of the Royal Society of London, B, 123*, 90–118.

Wijngaard, W. & van Kruysbergen, J. (1975). The function of the nonguided light in some explanations of the Stiles–Crawford effects. In Snyder, A. W. & Menzel, R. (Eds), *Photoreceptor optics* (pp. 175–183). Berlin: Springer.

Yasuma, T., Hamer, R. D., Lakshminarayanan, V., Enoch, J. M. & O'Donnell, J. J. (1986). Retinal receptor alignment and directional sensitivity in a gyrate atrophy patient. *Clinical Vision Sciences, 1*, 93–102.

Acknowledgements—The authors would like to thank Professor Rinaldo Alfieri and Dr Stephen Burns for their support and interest throughout this project. This work was supported by the CNRS (France), and by grants from the James H. & Alice Teubert Charitable Trust Foundation (U.S.A.) and from Essilor (France).